UNIVERSITAT POLITÈCNICA DE CATALUNYA

MASTER OF SCIENCE IN COMPUTATIONAL MECHANICS

DEPARTAMENT DE MATEMÀTICA APLICADA III

COMPUTATIONAL DYNAMIC SIMULATION OF BIOLOGICAL MEMBRANES

by BEHROOZ HASHEMIAN

Master Thesis

Advisor: Marino Arroyo

Barcelona, June 2010

Abstract

Computational Dynamic Simulation of Biological Membranes

Behrooz Hashemian

Biological membranes made out of lipid bilayers are the fundamental separation structure in cells and are crucial to maintain life. Many physiological processes rely on dramatic shape and topological changes (e.g. fusion, fission) of fluid membrane systems. Fluidity is key to the versatility and constant reorganization of lipid bilayers. Although the membrane intrinsic viscosity plays an important role in the dynamics of morphological changes of fluid vesicles, in the large vesicles, ambient bulk viscosity is dominant driving and dissipative mechanisms.

Here, a novel numerical technique is introduced in order to simulate the dynamic behavior of biological membranes immersed in a viscous, incompressible, Newtonian fluid. This method utilizes Finite Element Immersed Boundary (FEIB) method in combination with B-Spline curve representation and unlike the immersed boundary (IB) method consists of a variational formulation. The relaxation dynamics of fluid vesicles put in an out-of-equilibrium state is considered, and simulation is carried out regarding the kinetics of configuration changes in the membrane. Moreover, a special formulation, in which bulk dissipation matrix is derived, allows us to combine bulk dissipation with other dissipation mechanisms.

Keywords: Biological membranes; Fluid membranes; Finite Element Immersed Boundary (FEIB) method; B-Spline curve representation; Fluid-structure interaction; Helfrich-Canham functional.

Acknowledgments

First and foremost, I would like to thank my thesis advisor, Prof. Marino Arroyo, for sharing his knowledge, comments, suggestions and for his support during this investigation.

I would like to thank my professors at Universitat Politècnica de Catalunya and Swansea University for their broad perspective and abundant knowledge inspired me to study computational mechanics.

I want to express my gratitude towards my friends at LaCàN and CIMNE, and especially my colleagues at K2M, for their help, interest and valuable advice.

Finally, and most importantly, I would like to thank my family, my admirable father, compassionate mother and beloved brothers, for their unconditional support and motivation during my entire life.

Contents

List of Figures

Chapter 1

Introduction

1.1 Motivation

In the past few decades, numerous research efforts have been directed to method development for the modeling of fluid-structure interaction for biological systems (Liu et al., 2006). Numerical investigations of fluid-structure interaction problems require reliable numerical modeling and simulation tools (Belytschko, 1980; Liu et al., 1986). An efficient and robust modeling technique is essential in the study of complicated physical phenomena, especially in bioscience and biomedical fields. Biological membranes are crucial to the life of the cell and all biomembranes have the same basic phospholipid bilayer structure and certain common functions. These amphiphilic membranes are self-assembled structures made out of lipids or other amphiphilic molecules such as diblock co-polymers. Above a transition temperature, these membranes are fluid within the membrane surface, while they retain the transversal order, which confers them with bending rigidity. The membrane fluidity is essential for many biochemical processes involving membrane proteins (Saffman and Delbruck, 1975). It has been computationally and experimentally shown that even at very small scales, the motion of the amphiphilic molecules is due to collective two-dimensional flows rather than molecular diffusion (Shillcock and Lipowsky, 2006).

A number of theoretical models and simulation methods have been used to study fluid membranes (Arroyo and DeSimone, 2009). Atomistic molecular dynamics (MD)

simulations have been very useful in this and other respects, but remain limited to small membrane patches due to the prohibitive number of atoms involved in closed vesicles and the slow equilibration times of membrane systems (Gurtovenko and Vattulainen, 2005). Coarse-grained MD allows us to reach small closed vesicles, but suffers from the same fundamental difficulties (Shillcock and Lipowsky, 2006; Cooke et al., 2005; Reynwar et al., 2007). Continuum mechanics has proven very effective in describing the mechanics of membrane systems and reproducing both experimental and atomistic results (Danov et al., 2000; Dimova et al., 2006).

Among the computational methods developed for fluid-structure interactions, one of the most noticeable contributions is the immersed boundary (IB) method which was originally developed by Peskin for the computation of blood flows interacting with the heart and heart valves (Peskin, 1972). The mathematical formulation of the IB method employs a mixture of Eulerian and Lagrangian descriptions for fluid and solid domains. The interaction between fluid and solid domains is accomplished by distributing nodal forces and interpolating nodal velocities between Eulerian fluid and Lagrangian solid domains. The advantage of the IB method is that the fluid-structure interface is automatically tracked, which circumvents costly mesh updating algorithms.

Here, we are going to utilize a novel numerical method, named Finite Element Immersed Boundary (FEIB) Method (Heltai, 2008; Boffi et al., 2005), in combination with B-Spline curve representing geometry (Hughes et al., 2005) in order to simulate the behavior of a biological membrane immersed in a bulk fluid. This method is built based on the fundamental concepts of IB method, but eliminated the critical drawbacks of the IB method. Unlike the Dirac delta functions in the IB method which yield C^1 continuity (Peskin, 2003; Mittal and Iaccarino, 2005), the discretized delta function in IFEM is the C^n shape function. Another important feature of the presented numerical method is using the variational formulation.

Despite the morphology of fluid biomembrane systems is very dynamic, both in the cell and in synthetic systems, most continuum studies have concentrated on the equilibrium shapes and phase diagrams of vesicles. When studying the dynamics

with continuum mechanics models, the membrane viscosity has been traditionally disregarded or neglected. An important obstacle to bring into account the membrane dissipation mechanisms has been the complexity of the equations describing the viscous two-dimensional fluid flow of the amphiphiles on a curved time-evolving geometry. Here, we present the calculations coupling the two-dimensional flow of the amphiphiles on the membrane with the shape changes driven by curvature elasticity. These calculations are based on a finite element B-Spline approximation for both the shape and the membrane fluid flow equations.

1.2 Outline

In the next chapter (Chapter 2), the biological membranes are explained from the molecular biology point of view. Their basic biological composition and structure are discussed, and the physical role of lipids on fluidity and bilayer formation are argued.

In Chapter 3, a continuum model is introduced for the biological membranes. The biological membrane is considered as an inextensible fluid membrane with curvature elasticity immersed in a viscous, incompressible, Newtonian fluid. Different dissipation models are described and finally Helfrich-Canhm curvature energy is discussed and its derivatives are derived.

In Chapter 4 a combined method using finite element immersed boundary method (FEIB) and B-Spline curves representation is introduced. A special semi-discretization is described and the bulk dissipation matrix is calculated. At last, an effective re-parametrization method in order to increase the accuracy of geometry and avoid undesirable clustering of control points is introduced.

Chapter 5 is devoted to show the final dynamic simulation results of biological membranes as well as verifying the numerical method with analytical solution of the most important example of an asymmetrical flow (Happel and Brenner, 1983).

Chapter 2

Biological Membranes

2.1 Introduction

Biological membranes are crucial to the life of the cell. Although all biomembranes have the same basic phospholipid bilayer structure and certain common functions, each type of cellular membranes also has certain distinctive activities determined largely by the unique set of proteins associated with that membrane (Lodish et al., 2003). In this chapter, we, first, discuss the basic biological composition and structure of all biological membranes with emphasis on the lipid bilayers. Next, we outline functions of the plasma membrane in cell organisms, and then argue the physical role of lipids on fluidity and bilayer formation.

2.2 Biological Composition and Structure

Biomembranes enclose the cell, define its boundaries, and maintain the essential differences between the cytosol and the extracellular environment, see figure 2.1. Despite their differing functions, all biological membranes have a common general structure: each is very thin film of lipid and protein molecules, held together mainly by non-covalent interactions. Biological membranes are dynamics, fluid structures, and most of their molecules move about in the plane of the membrane. The lipid molecules are arranged as a continuous double layer about 5nm thick. This *lipid bilayer* provides the

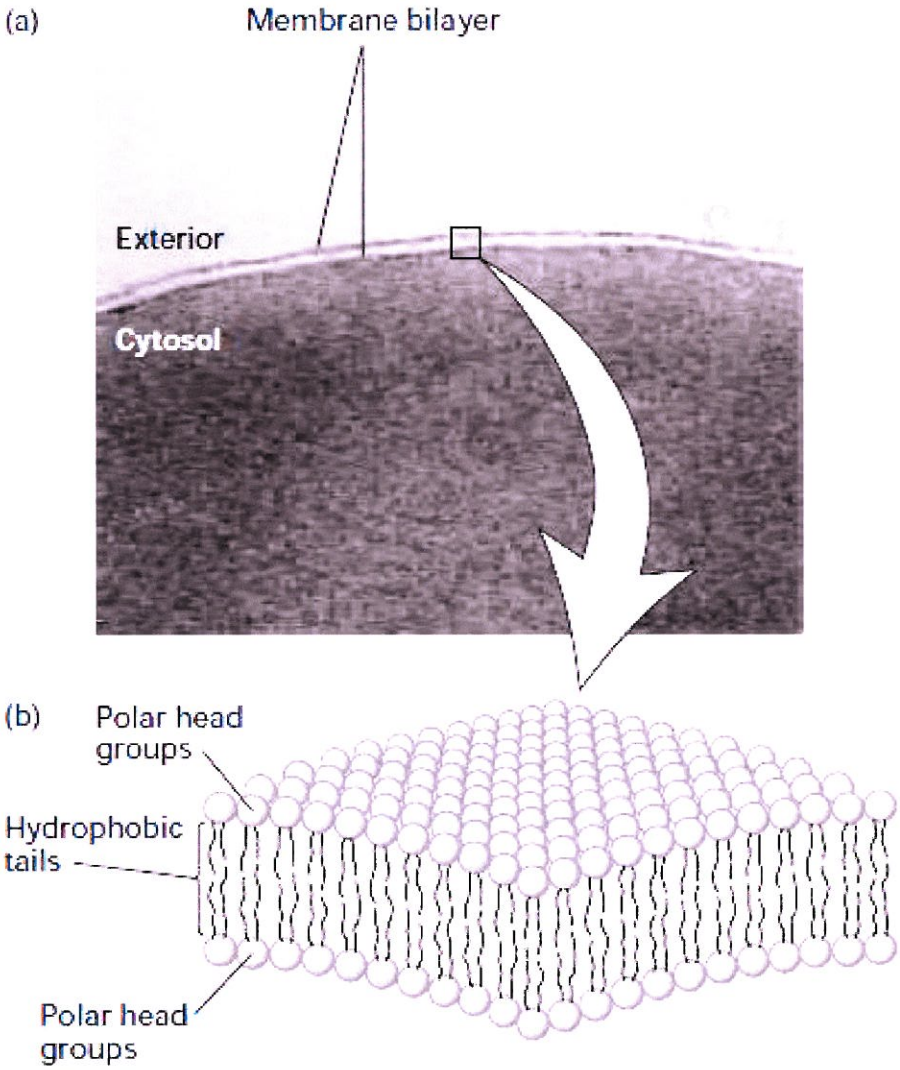

Figure 2.1: The bilayer structure of biomembranes. (a) Electron micrograph of a thin section through an erythrocyte membrane. The characteristic "railroad track" appearance of the membrane indicates the presence of two polar layers, consistent with the bilayer structure for phospholipid membranes. (b) Schematic interpretation of the phospholipid bilayer in which polar groups face outward to shield the hydrophobic tails from water. The hydrophobic effect and van der Waals interactions between the tails drive the assembly of the bilayer (Lodish et al., 2003)

basic fluid structure of the membrane and serves as a relatively impermeable barrier to the passage of most water-soluble molecules.

2.2.1 The Lipid Bilayer

The lipid bilayer provides the basic structure for all biomembranes and has two important properties. First, the hydrophobic core is an impermeable barrier that prevents the diffusion of water-soluble (hydrophilic) solutes across the membrane. Importantly, this simple barrier function is modulated by the presence of membrane proteins that mediate the transport of specific molecules across this otherwise impermeable bilayer. The second property of the bilayer is its stability and its structure is maintained by hydrophobic and van der Waals interactions between the lipid chains. Even though the exterior aqueous environment can vary widely in ionic strength and pH, the bilayer has the strength to retain its characteristic architecture.

Three major classes of lipids can be found in a typical biomembrane: phosphoglycerides, sphingolipids, and steroids. All of them are amphipathic molecules having a polar (hydrophilic) head group and hydrophobic tail. The hydrophobic effect and van der Waals interactions cause the tail groups to self-associate into a bilayer with the polar head groups oriented toward water (figure 2.1). Although the common membrane lipids have this amphipathic character in common, they differ in their chemical structures, abundance, and functions in the membrane.

Phosphoglycerides, the most abundant class of lipids in most membranes, are derivatives of glycerol 3-phosphate (figures 2.2 and 2.3a). A typical phosphoglyceride molecule consists of a hydrophobic tail composed of two fatty acyl chains esterified to the two hydroxyl groups in glycerol phosphate and a polar head group attached to the phosphate group. The two fatty acyl chains may differ in the number of carbons that they contain (commonly 16 or 18) and their degree of saturation (0, 1, or 2 double bonds). A phosphoglyceride is classified according to the nature of its head group. In phosphatidylcholines, the most abundant phospholipids in the plasma membrane, the head group consists of choline, a positively charged alcohol, esterified to the negatively charged phosphate. In other phosphoglycerides, an OH-containing molecule such as serine, ethanolamine, and the sugar derivative inositol is linked to the phosphate group. The negatively charged phosphate group and the positively charged groups or the hydroxyl groups on the head group interact strongly with water.

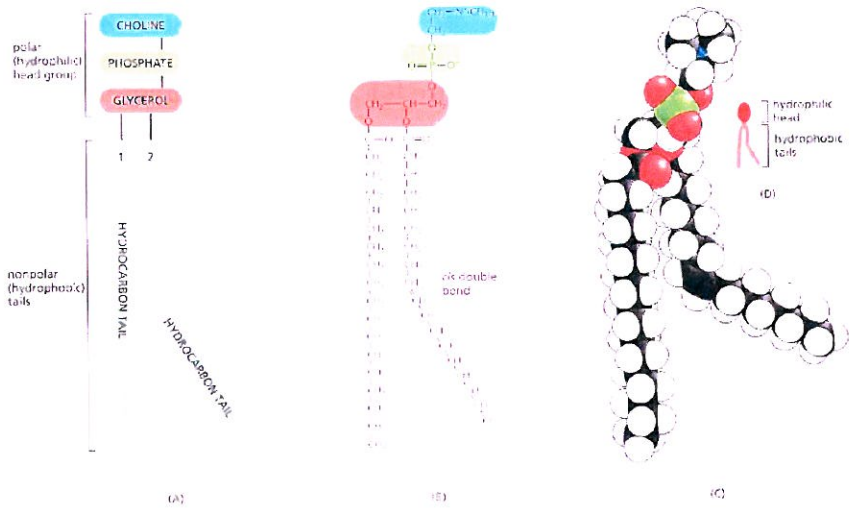

Figure 2.2: The parts of a phosphoglyceride molecule. (A) Schematically, (B)by a formula, (C)as a space-filling model, and (D)as a symbol (Alberts, 1998).

A second class of membrane lipid is the **sphingolipids**. In sphingomyelin, the most abundant sphingolipid, phosphocholine is attached to the terminal hydroxyl group of sphingosine (Figure 2.3b). Thus sphingomyelin is a phospholipid, and its overall structure is quite similar to that of phosphatidylcholine. Glucosylcerebroside, the simplest glycosphingolipid, contains a single glucose unit attached to sphingosine. In the complex glycosphingolipids called gangliosides, one or two branched sugar chains containing sialic acid groups are attached to sphingosine. Glycolipids constitute 2–10 percent of the total lipid in plasma membranes; they are most abundant in nervous tissue.

Cholesterol and its derivatives constitute the third important class of membrane lipids, the **steroids**. The basic structure of steroids is a four-ring hydrocarbon. Cholesterol, the major steroidal constituent of animal tissues, has a hydroxyl substituent on one ring (figure 2.3c). Although cholesterol is almost entirely hydrocarbon in composition, it is amphipathic because its hydroxyl group can interact with water. Cholesterol is especially abundant in the plasma membranes of mammalian cells but is absent from most prokaryotic cells.

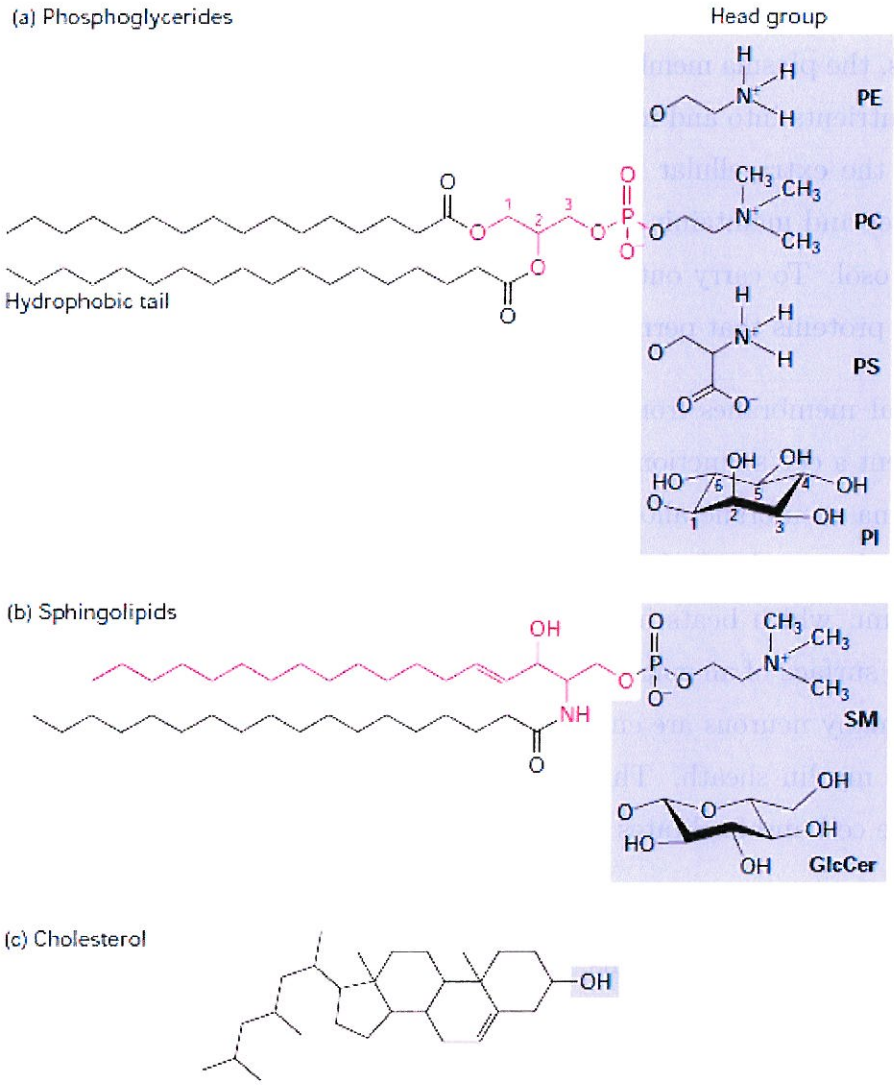

Figure 2.3: Three classes of membrane lipids. (a) Most phosphoglycerides are derivatives of glycerol 3-phosphate (red) containing two esterified fatty acyl chains, constituting the hydrophobic tail and a polar head group esterified to the phosphate. (b) Sphingolipids are derivatives of sphingosine (red), an amino alcohol with a long hydrocarbon chain. (c) Like other membrane lipids, the steroid cholesterol is amphipathic. Its single hydroxyl group is equivalent to the polar head group in other lipids; the conjugated ring and short hydrocarbon chain form the hydrophobic tail(Sprong et al., 2001).

2.2.2 Functionality of the Plasma Membrane

In all cells, the plasma membrane has several essential functions. These include transporting nutrients into and metabolic wastes out of the cell; preventing unwanted materials in the extracellular milieu from entering the cell; preventing loss of needed metabolites and maintaining the proper ionic composition, pH, and osmotic pressure of the cytosol. To carry out these functions, the plasma membrane contains specific transport proteins that permit the passage of certain small molecules but not others.

Natural membranes from different cell types exhibit a variety of shapes, which complement a cell's function (Figure 2.4). The smooth flexible surface of the erythrocyte plasma membrane allows the cell to squeeze through narrow blood capillaries. Some cells have a long, slender extension of the plasma membrane, called a cilium or flagellum, which beats in a whip-like manner. This motion causes fluid to flow across the surface of an epithelium or a sperm cell to swim through the medium. The axons of many neurons are encased by multiple layers of modified plasma membrane called the myelin sheath. This membranous structure is elaborated by an adjacent supportive cell and facilitates the conduction of nerve impulses over long distances.

In addition to these universal functions, the plasma membrane has other critical roles in multicellular organisms. Few of the cells in multicellular plants and animals exist as isolated entities; rather, groups of cells with related specializations combined to form tissues. Specialized areas of the plasma membrane contain proteins and glycolipids that form specific contacts and junctions between cells to strengthen tissues and to allow the exchange of metabolites between cells. Proteins in the plasma membrane anchor cells to many of the matrix components, adding to the strength and rigidity of many tissues. In addition, enzymes bound to the plasma membrane catalyze reactions that would occur with difficulty in an aqueous environment. The plasma membrane of many types of eukaryotic cells also contains receptor proteins that bind specific signaling molecules (e.g. hormones, growth factors, and neurotransmitters), leading to various cellular responses.

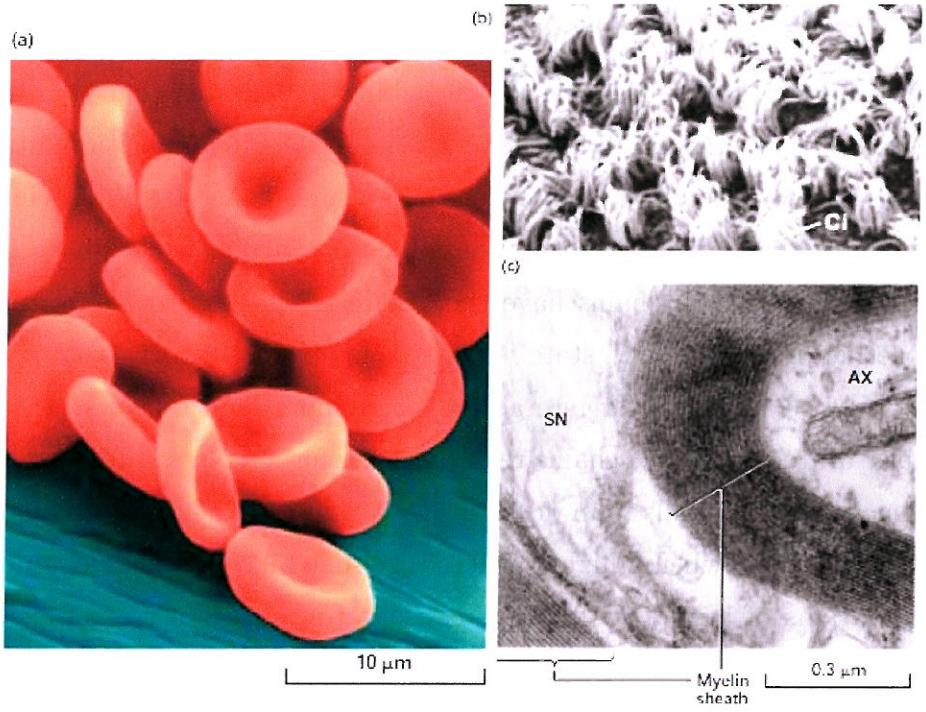

Figure 2.4: Variation in biomembranes in different cell types. (a) A smooth, flexible membrane covers the surface of the discoid erythrocyte cell. (b) Tufts of cilia (Ci) project from the ependymal cells that line the brain ventricles. (c) Many nerve axons are enveloped in a myelin sheath composed of multiple layers of modified plasma membrane. [Parts (a) and (b) from Kessel and Kardon (1979), and (c) from Cross and Mercer (1993)]

2.3 Physical Role of Lipids

The ability of individual lipid molecules to diffuse freely within lipid bilayers results the fluidity of bilayers. Despite this fluidity, lipid bilayers can form domain of different compositions. However not all lipids can form bilayers while the formation depends on the solubility and the shape of lipid molecules.

2.3.1 Fluidity

The ability of lipids to diffuse laterally in a bilayer indicates that it can act as a fluid. The degree of bilayer fluidity depends on the lipid composition, structure of the phospholipid hydrophobic tails, and temperature. Van der Waals interactions and the hydrophobic effect cause the nonpolar tails of phospholipids to aggregate. Long, saturated fatty acyl chains have the greatest tendency to aggregate, packing tightly together into a gel-like state. Phospholipids with short fatty acyl chains, which have less surface area for interaction, form more fluid bilayers. Likewise, the links in unsaturated fatty acyl chains result in their forming less stable van der Waals interactions with other lipids than do saturated chains and hence more fluid bilayers. As shown in figure 2.5 when a highly ordered, gel-like bilayer is heated, the increased molecular motions of the fatty acyl tails cause it to undergo a transition to a more fluid, disordered state.

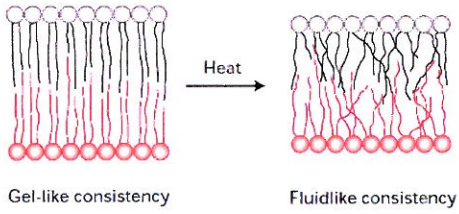

Figure 2.5: Gel and fluid forms of the phospholipid bilayer. Heat disorders the nonpolar tails and induces a transition from a gel to a fluid within a temperature range of only a few degrees. (Alberts et al., 2007).

2.3.2 Bilayer Formation

Two factors primarily govern whether a lipid will form a bilayer or not: solubility and shape. For a self-assembled structure such as a bilayer to form, the lipid should have a low solubility in water, which can determined by critical micelle concentration (CMC) (Israelachvili, 1991). Above the CMC, molecules will aggregate and form larger structures such as bilayers, micelles or inverted micelles.

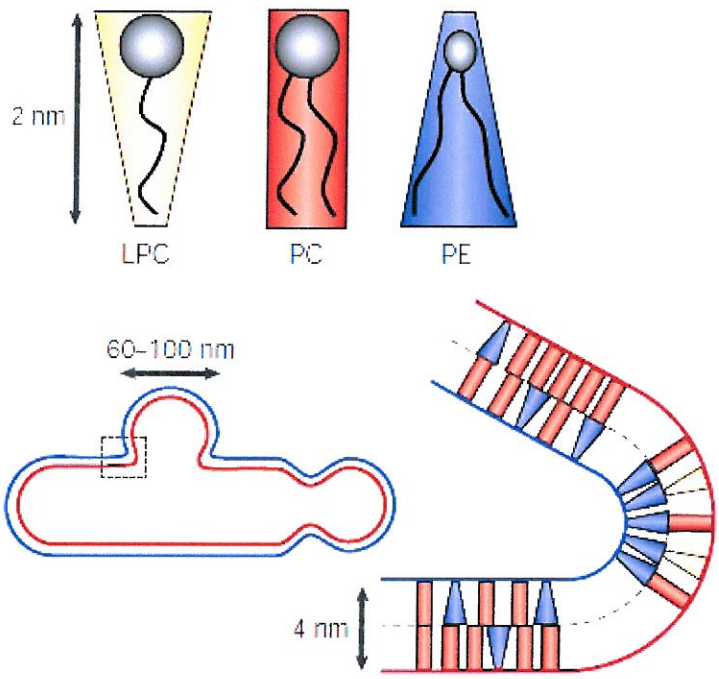

Figure 2.6: The molecular shape of lipids (Sprong et al., 2001).

The shape of a membrane lipid depends on the relative size of its polar headgroup and apolar tails (Cullis et al., 1986). As shown in figure 2.6, the molecular shape of lipids determines the physical properties of membranes. In cases in which the headgroup and lipid backbone have similar cross-sectional areas, the molecule has a cylindrical shape (phosphatidylcholine (PC)). Lipids with a small headgroup like phosphatidylethanolamine (PE) are cone-shaped. By contrast, when the hydrophobic part occupies a relatively smaller surface area, the molecule has the shape of an inverted cone (lysophosphatidylcholine (LPC)). The relative size of polar headgroup to apolar tails can be used to define so-called **intrinsic curvature**. For two-tailed PC lipids, this ratio is nearly one so the intrinsic curvature is nearly zero. PE lipids are smaller and the resulting diacyl (two-tailed) lipids thus have negative intrinsic curvature. LPC lipids tend to have positive spontaneous curvature because they have one (rather than two) alkyl chain in the tail region. If a particular lipid has too large deviation from zero intrinsic curvature, it will not form a bilayer.

Chapter 3

Mathematical Formulation

3.1 Introduction

In this chapter, a continuum model is introduced for the biological membranes; this model considers a biological membrane as an inextensible fluid membrane with curvature elasticity immersed in a viscous, incompressible, Newtonian fluid. The inertial forces are ignored and the biomembrane is modeled as a Newtonian two-dimensional fluid, in agreement with coarse-grained molecular dynamics simulations (den Otter and Shkulipa, 2007) and experimental observations (Danov et al., 2000; Dimova et al., 2006; Cicuta et al., 2007). Here, first we describe the kinematics which is in a Lagrangian system and then discuss the dissipation energies and curvature elasticity.

3.2 Kinematics

We describe parametrically axisymmetric vesicles in terms of the generating curve, i.e. the vesicle surface Γ_t at a given instant t is given by

$$\boldsymbol{x}(u,\theta;t) = \{r(u;t)\cos\theta, r(u;t)\sin\theta, z(u;t)\}, \qquad u \in [0,1],\ \theta \in [0,2\pi],$$

where

$$\boldsymbol{c}(u;t) = \{r(u;t), z(u;t)\}, \qquad u \in [0,1],$$

is the parametric description of the generating curve at the instant t, $\mathcal{C}_t$. We consider closed surfaces with continuous tangents, hence we require

$$r(0) = r(1) = 0, \qquad z'(0) = z'(1) = 0, \tag{3.1}$$

where $(\cdot)'$ denotes partial differentiation with respect to u.

For simplicity, from this point on we omit the dependence of all quantities on time. We shall formulate the mechanics of the fluid membrane in terms of the generating curve. Its speed is given by $a(u) = \sqrt{[r'(u)]^2 + [z'(u)]^2}$. Integrals on the surface can be brought to the interval $[0, 1]$ with the relation $\mathrm{d}S = (2\pi ar)\mathrm{d}u$. The tangent unit vector to the generating curve pointing in the u direction and a unit normal are given by

$$\boldsymbol{t} = \frac{1}{a}\{r', z'\}, \qquad \boldsymbol{n} = \frac{1}{a}\{-z', r'\}.$$

Viewing the parameter u as a label for material particles, we can express the velocity of the membrane in terms of its tangential and normal components,

$$\dot{\boldsymbol{c}} = \{\dot{r}, \dot{z}\} = \boldsymbol{V} = \boldsymbol{v} + v_n\boldsymbol{n} = v_t\boldsymbol{t} + v_n\boldsymbol{n},$$

where the dot denotes partial differentiation with respect to time, $\boldsymbol{v}$ is tangential component and

$$v_t = \frac{1}{a}(r'\dot{r} + z'\dot{z}), \qquad v_n = \frac{1}{a}(-z'\dot{r} + r'\dot{z}). \tag{3.2}$$

This decomposition is important since only the normal velocities change the shape of the membrane. The tangential velocities represent the flow of the amphiphiles on the membrane surface. The above relations can be inverted as

$$\dot{r} = \frac{1}{a}(r'v_t - z'v_n), \qquad \dot{z} = \frac{1}{a}(r'v_n + z'v_t).$$

A key object for the kinematics and constitutive relations of the two-dimensional fluid on a curved, time-evolving surface is the rate-of-deformation tensor $\boldsymbol{d}$. This tensor

can be geometrically thought as the tangent projection of the rate of change of the metric tensor of the surface as it is advected by the membrane velocity (Scriven, 1960; Marsden and Hughes, 1983; Arroyo and DeSimone, 2009), which leads to the expression

$$\boldsymbol{d} = \frac{1}{2}\left(\boldsymbol{\nabla}_s \boldsymbol{v} + \boldsymbol{\nabla}_s \boldsymbol{v}^T\right) - v_n \boldsymbol{k},$$

where $\boldsymbol{\nabla}_s$ denotes the surface covariant derivative and $\boldsymbol{k} = -\boldsymbol{\nabla}_s \boldsymbol{n}$ the second fundamental form. The formulas for axisymmetric surfaces can be found in Arroyo and DeSimone (2009).

Introducing $b(u) = -r''(u)z'(u) + r'(u)z''(u)$, we can write the mean and gaussian curvatures as

$$H = \frac{1}{a}\left(\frac{b}{a^2} + \frac{z'}{r}\right), \qquad K = \frac{bz'}{a^4 r}. \tag{3.3}$$

Note that here H is defined as the trace of the second fundamental form.

3.3 Governing Equations

Hre, We present the generic ingredients for the governing equations for the shape evolution, under the assumption of low Reynolds number, hence neglecting inertia. The dissipative potentials can be expressed by a functional $W[\dot{r}, \dot{z}]$, which, although not explicitly written, depends nonlinearly on the shape of the surface. Under the assumption that both the ambient bulk fluid and the membrane two-dimensional fluid are Newtonian, this functional is quadratic in its arguments.

The curvature energy and in general other energetic mechanisms such as line tension, depend exclusively on the shape of the membrane, hence can be expressed in terms of a nonlinear functional $\Pi[r, z]$. The energy release rate functional is the negative of the variation of the energy functional in the direction of $\{\dot{r}, \dot{z}\}$, i.e. $G[\dot{r}, \dot{z}] = -\delta\Pi[r, z; \dot{r}, \dot{z}]$, where again its explicit (nonlinear) dependence on the configuration of the surface has been omitted. By its definition, it is clear that the energy release rate functional is linear in its arguments.

The membrane dynamics are often constrained by global nonlinear equalities such

as enclosed volume or surface area constraints. We generically express these constraints with a vector-valued functional as $\boldsymbol{C}[r,z]=\mathbf{0}$, or in rate form as $\boldsymbol{D}[\dot{r},\dot{z}]=\delta\boldsymbol{C}[r,z;\dot{r},\dot{z}]=\mathbf{0}$. Again, this functional is linear in its arguments and nonlinear in the configuration of the membrane. We shall also consider local constraints such as the local inextensibility of the membrane, expressed at each point of the membrane as $d(\dot{r},\dot{z})=0$.

The dynamics of the membrane equilibrates the dissipative and the energetic forces subject to the constraints. Mathematically, the evolution equations follow from minimizing $W[\dot{r},\dot{z}]-G[\dot{r},\dot{z}]$ subject to the constraints. Forming the Lagrangian

$$\mathcal{L}[\dot{r},\dot{z},\lambda,\boldsymbol{\Lambda}]=W[\dot{r},\dot{z}]-G[\dot{r},\dot{z}]-\int_{\Gamma}\lambda d(\dot{r},\dot{z})\mathrm{d}S-\boldsymbol{\Lambda}\cdot\boldsymbol{D}[\dot{r},\dot{z}],$$

we find the velocities at each configuration $\{r,z\}$, finding the stationary points with respect to all admissible variations

$$\delta_{\dot{r}}\mathcal{L}=\delta_{\dot{z}}\mathcal{L}=\delta_{\lambda}\mathcal{L}=\delta_{\boldsymbol{\Lambda}}\mathcal{L}=0, \tag{3.4}$$

which is a form of the principle of virtual power. Note that, unlike the other arguments of the Lagrangian functional, the Lagrange multipliers for the global constraints $\boldsymbol{\Lambda}$ are not functions of u. If $d(\dot{r},\dot{z})=0$ expresses the local inextensibility of the membrane, then the Lagrange multiplier λ is the surface tension. We provide below the specific form of these functionals.

3.4 Constraints

Fluid membranes are semipermeable, and assuming osmotic equilibrium between the enclosed and the outer media, it is often reasonable to assume that the enclosed

volume is constant. This constraint is expressed as

$$0 = D^{\text{vol}}[\dot{r}, \dot{z}] = \dot{V} = -\int_\Gamma v_n \mathrm{d}S = -\int_0^1 \frac{1}{a}(-z'\dot{r} + r'\dot{z})(2\pi a r)\mathrm{d}u. \tag{3.5}$$

Generally, the in-plane stresses on the membrane are low compared to the elastic moduli, and the membrane can be assumed to be locally inextensible (Seifert and Lipowsky, 1995). This condition on the surface is expressed as (Arroyo and DeSimone, 2009)

$$0 = \text{trace } \boldsymbol{d} = \boldsymbol{\nabla}_s \cdot \boldsymbol{v} - H v_n,$$

which for axisymmetric surfaces reduces to

$$0 = d^{\text{inext}}(\dot{r}, \dot{z}) = \frac{1}{ar}(r v_t)' - H v_n = \left(\frac{r'}{a^2} - \frac{H z'}{a}\right)\dot{r} + \left(\frac{z'}{a^2} + \frac{H r'}{a}\right)\dot{z}.$$

If the details of the fluid flow on the membrane are disregarded, this local condition is often replaced by a total surface area constraint (Du et al., 2009), which for a closed surface takes the form

$$0 = D^{\text{area}}[\dot{r}, \dot{z}] = \dot{S} = -\int_\Gamma H v_n \mathrm{d}S = -\int_0^1 \frac{H}{a}(-z'\dot{r} + r'\dot{z})(2\pi a r)\mathrm{d}u. \tag{3.6}$$

3.5 Dissipation

3.5.1 Membrane Dissipation

As derived in Arroyo and DeSimone (2009), the dissipation potential for a Newtonian closed fluid membrane can be written as

$$\begin{aligned} W^{\text{mem}}[\boldsymbol{v}, v_n] &= \int_\Gamma \mu\, \boldsymbol{d} : \boldsymbol{d}\, \mathrm{d}S \\ &= \int_\Gamma \mu \left[\frac{1}{2}|\mathrm{d}\boldsymbol{v}^\flat|^2 + (\boldsymbol{\nabla}_s \cdot \boldsymbol{v})^2 - K|\boldsymbol{v}|^2 + (H^2 - 2K)v_n^2 - 2(\boldsymbol{\nabla}_s \boldsymbol{v} : \boldsymbol{k})v_n\right] \mathrm{d}S, \end{aligned}$$

where $\mathbf{d}$ denotes the exterior derivative, $\mathbf{d}\boldsymbol{v}^\flat$ is the generalization of the curl of the tangent velocity field on the surface, and μ denotes the membrane viscosity, with units of force $\times$ time $\times$ length^{-1}. Molecular dynamics simulations (den Otter and Shkulipa, 2007) as well as experiments (Danov et al., 2000; Dimova et al., 2006) support modeling fluid membranes as Newtonian two-dimensional fluids. For axisymmetric surfaces, this expression reduces to

$$\begin{aligned} W^{\text{mem}}[\dot{r},\dot{z}] &= \int_\Gamma \mu \left[\left(\frac{1}{a}v_t'\right)^2 + \left(\frac{r'}{ar}v_t\right)^2 - \frac{2}{a}v_n\left(\frac{b}{a^3}v_t' + \frac{z'r'}{ar^2}v_t\right) + (H^2-2K)v_n^2 \right] \mathrm{d}S, \\ &= \int_\Gamma \mu \begin{bmatrix} v_t' & v_t & v_n \end{bmatrix} \begin{bmatrix} \frac{1}{a^2} & 0 & -\frac{b}{a^4} \\ 0 & \left(\frac{r'}{ar}\right)^2 & -\frac{z'r'}{(ar)^2} \\ -\frac{b}{a^4} & -\frac{z'r'}{(ar)^2} & H^2-2K \end{bmatrix} \begin{bmatrix} v_t' \\ v_t \\ v_n \end{bmatrix} \mathrm{d}S. \end{aligned}$$

The matrix in the above expression is positive semidefinite. Indeed, it becomes obvious from the derivations that it has a zero eigenvalue associated with rigid body motions, i.e. velocity fields obtained from equation (3.2) and $\dot{r} = 0$ and $\dot{z} =$ constant. This reflects the fact that the membrane dissipation is internal to the surface.

We provide here a remarkably simple alternative expression of this dissipation potential under the hypothesis of axisymmetry. We first use the the local inextensibility constraint to express v_t' in terms of v_t and v_n. The dissipation potential then takes the form

$$W^{\text{mem}}[\dot{r},\dot{z}] = \int_\Gamma \mu \frac{2}{(ar)^2} \begin{bmatrix} v_t & v_n \end{bmatrix} \begin{bmatrix} (r')^2 & -r'z' \\ -r'z' & (z')^2 \end{bmatrix} \begin{bmatrix} v_t \\ v_n \end{bmatrix} \mathrm{d}S,$$

which, using equation (3.2), can be written as

$$W^{\text{mem}}[\dot{r},\dot{z}] = \int_\Gamma 2\mu \left(\frac{\dot{r}}{r}\right)^2 \mathrm{d}S = \int_0^1 2\mu \left(\frac{\dot{r}}{r}\right)^2 (2\pi ar)\mathrm{d}u. \tag{3.7}$$

3.5.2 Bulk Dissipation

We assume that the velocities of the membrane and of the surrounding fluid coincide, i.e. no slip as suggested by coarse-grained MD simulation (den Otter and Shkulipa, 2007) and conventionally assumed for lipid-water interactions (Stone and Ajdari, 1998). This hypothesis may not be adequate in extreme situations, for instance if there is significant flow across the membrane. We consider an infinite fluid at rest at infinity and axisymmetry.

In the absence of body forces, the dissipation potential can be written as

$$W^{\text{bulk}} = \frac{1}{2}\int_{\mathbb{R}^3} \boldsymbol{\sigma} : D \, \mathrm{d}V = \int_{\mathbb{R}^3} \mu^{\text{bulk}} D : D \, \mathrm{d}V,$$

where $\boldsymbol{\sigma}$ is the stress tensor, $D = 1/2[\boldsymbol{\nabla u} + (\boldsymbol{\nabla u})^T]$ the rate-of-deformation tensor in the bulk fluid, and $\boldsymbol{u}$ denotes the velocity field of the bulk fluid. This fluid is assumed to be incompressible, $\boldsymbol{\nabla} \cdot \boldsymbol{u} = 0$. The no-slip condition is expressed as $\boldsymbol{u} = \boldsymbol{V}$ on Γ.

3.6 Curvature Elasticity

The curvature elasticity of the fluid membrane is modeled by the Helfrich-Canham functional (see Seifert and Lipowsky, 1995, for a discussion on curvature elasticity models),

$$\Pi = \int_\Gamma \frac{\kappa}{2}(H - C_0)^2 \, dS + \int_\Gamma \kappa_G K \, \mathrm{d}S, \tag{3.8}$$

where C_0 denotes the spontaneous curvature and κ and κ_G are elastic parameters. For closed homogeneous surfaces, the second term is a topological invariant, which we will disregard here. For a general treatment for membranes with boundary, see Arroyo and DeSimone (2009). The energy release rate takes the form

$$G[v_n] = -\int_\Gamma \kappa(H - C_0)\left[\Delta_s v_n + \frac{1}{2}\left(H^2 - 4K + HC_0\right) v_n\right] \mathrm{d}S.$$

For the numerical implementation, to avoid third order derivatives of r and z, it proves more convenient to take variations directly from the following form of the elastic energy

$$\Pi[r,z] = \int_0^1 \frac{\kappa}{2}(H - C_0)^2 (2\pi a r)\mathrm{d}u, \tag{3.9}$$

together with equation (3.3), which yields an expression for $G[\dot{r},\dot{z}]$ as follows.

$$G[\dot{r},\dot{z}] = -\int_0^1 \kappa(H-C_0)\left(\frac{\partial H}{\partial r}\dot{r} + \frac{\partial H}{\partial r'}\dot{r}' + \frac{\partial H}{\partial r''}\dot{r}'' + \frac{\partial H}{\partial z'}\dot{z}' + \frac{\partial H}{\partial z''}\dot{z}''\right)(2\pi a r)\mathrm{d}u$$
$$+ \int_0^1 \kappa(H-C_0)^2\left(\frac{r'}{a}\dot{r}' + \frac{z'}{a}\dot{z}' + a\dot{r}\right)\pi\mathrm{d}u,$$

where

$$\frac{\partial H}{\partial r} = -\frac{z'}{ar^2}, \quad \frac{\partial H}{\partial r'} = \frac{z''}{a^3} - \frac{3br'}{a^5}, \quad \frac{\partial H}{\partial r''} = -\frac{z'}{a^3}, \quad \frac{\partial H}{\partial z'} = -\frac{r''}{a^3} - \frac{3bz'}{a^5} + \frac{1}{ar}, \quad \frac{\partial H}{\partial z''} = \frac{r'}{a^3}.$$

Both approaches can be shown to be equivalent by integration by parts with the conditions in equation (3.1) to annihilate the boundary terms.

3.7 Different Models

Here, we consider several models to assess the specific effects of the membrane viscous flow and its relevance. Initially, for the sake of qualitative comparison, we consider a model with only membrane dissipation, and local membrane inextensibility

$$\mathcal{L}^A[\dot{r},\dot{z},\lambda,\Lambda^{\mathrm{vol}}] = W^{\mathrm{mem}}[\dot{r},\dot{z}] - G[\dot{r},\dot{z}] - \int_\Gamma \lambda d^{\mathrm{inext}}(\dot{r},\dot{z})\mathrm{d}S - \Lambda^{\mathrm{vol}} D^{\mathrm{vol}}[\dot{r},\dot{z}].$$

We consider also a model with only bulk dissipation, together with a global area constraint as in Du et al. (2009)

$$\mathcal{L}^B[\dot{r}, \dot{z}, \Lambda^{\text{area}}, \Lambda^{\text{vol}}] = W^{\text{bulk}}[\dot{r}, \dot{z}] - G[\dot{r}, \dot{z}] - \Lambda^{\text{area}} D^{\text{area}}[\dot{r}, \dot{z}] - \Lambda^{\text{vol}} D^{\text{vol}}[\dot{r}, \dot{z}].$$

A similar model with local inextensibility can be considered, as in Biben et al. (2005). We have checked that the results for both models are very close, hence consider only $\mathcal{L}^B$ for definiteness.

We also consider a model whose dissipative mechanism is purely mathematical

$$\mathcal{L}^C[\dot{r}, \dot{z}, \Lambda^{\text{area}}, \Lambda^{\text{vol}}] = W^{L_2}[\dot{r}, \dot{z}] - G[\dot{r}, \dot{z}] - \Lambda^{\text{area}} D^{\text{area}}[\dot{r}, \dot{z}] - \Lambda^{\text{vol}} D^{\text{vol}}[\dot{r}, \dot{z}],$$

where

$$W^{L_2}[\dot{r}, \dot{z}] = \int_\Gamma \frac{\hat{\mu}}{2} v_n^2 \mathrm{d}S,$$

and $\hat{\mu}$ is a mathematical viscosity coefficient. The resulting dynamics, for the closed surfaces considered here, are a constrained version of the L_2 gradient flow of the Willmore energy. Such a gradient flow finds applications in geometrical analysis (Simonett, 2001), and is also considered by some authors as a simple model for the dynamics of fluid membranes (Du et al., 2006). In all the models presented so far, vesicles of different sizes evolve in the exact same way, upon re-scaling of the time variable. Finally, the following model accounts for both the membrane and the bulk dissipation

$$\mathcal{L}^{\text{full}}[\dot{r}, \dot{z}, \lambda, \Lambda^{\text{vol}}] = W^{\text{mem}}[\dot{r}, \dot{z}] + W^{\text{bulk}}[\dot{r}, \dot{z}] - G[\dot{r}, \dot{z}] - \int_\Gamma \lambda d^{\text{inext}}(\dot{r}, \dot{z}) \mathrm{d}S - \Lambda^{\text{vol}} D^{\text{vol}}[\dot{r}, \dot{z}].$$

In this model, the two dissipative mechanisms compete, and vesicles of different sizes exhibit a different relaxation behavior, as reported in Arroyo and DeSimone (2009).

These models could be supplemented by external actions, although here we only consider the relaxation dynamics from an initial out-of-equilibrium condition. Here, the out-of-equilibrium configurations are obtained as equilibria for a given value of

the spontaneous curvature C_0, which in the dynamics simulation is set to zero, or by applying an external force on the vesicle, which is suddenly released so that the systems returns to an equilibrium state. It should be mentioned that, while for models $\mathcal{L}^B$, $\mathcal{L}^C$, and $\mathcal{L}^{\text{full}}$ the boundary conditions in equation (3.1) are sufficient, the model $\mathcal{L}^A$ requires an additional condition to fix the motion along z, which otherwise remains undetermined due to the invariance of W^{mem} apparent from equation (3.7).

Chapter 4

Numerical Methods

4.1 Introduction

One of the most demanding methods to simulate the fluid-structure interaction in biological systems is the finite element immersed boundary (FEIB) method, see Heltai (2008); Boffi et al. (2005). This is a newly developed method based on the immersed boundary (IB) methods, firstly introduced by peskin in 1972 (Peskin, 1972) and widely used in fluid-membrane interaction problems Peskin (2003); Mittal and Iaccarino (2005). There are a considerable number of methods based on IB, such as Immersed Finite Element Method (IFEM), which have fundamental differences in formulation and application (Zhang et al., 2004; Liu et al., 2006, 2007; Zhilin, 1998). Here, we develop a new approach by utilizing FEIB and B-Spline curve representing geometry of biological membrane. In this chapter, a special semi-discretization, in which a Lagrangian B-Spline curve moves on top of a background Eulerian fluid mesh which spans the entire computational domain, is described and the bulk dissipation matrix is calculated. At last, in order to minimize the number of control points of the B-Spline while representing high curvatures more accurately and also avoiding undesirable control point clustering in some areas, an effective combined re-parametrization method is introduced.

4.2 Spacial Semi-discretization

The spacial discretization follows from a standard Galerkin approach. The generating curve of the axisymmetric surface is represented numerically as a B-Spline curve

$$\boldsymbol{c}(u;t) = \{r(u;t), z(u;t)\} \approx \sum_{I=1}^{N} B_I(u) \underbrace{\{r_I(t), z_I(t)\}}_{\boldsymbol{P}_I(t)}, \tag{4.1}$$

where $B_I(u)$ are the B-Spline basis functions (Piegl and Tiller, 1997) defined on the interval $[0, 1]$, and $\{r_I(t), z_I(t)\}$ is the position of the $I-$th control point of the B-Spline curve at instant t. Again, we drop the dependence on time. The velocity of the membrane can be computed as

$$\boldsymbol{V}(u) \approx \sum_{I=1}^{N} B_I(u) \dot{\boldsymbol{P}}_I. \tag{4.2}$$

Since the formulation involves up to second derivatives of the generating curve, it is convenient that the numerical representation is sufficiently smooth, hence avoiding cumbersome mixed approaches. Here, we have considered cubic B-Splines, which have up to second-order continuous derivatives. With the natural numbering of the basis functions, the symmetry conditions in equation (3.1) can be expressed in this numerical representation as $r_1 = r_N = 0$, $z_1 = z_2$ and $z_{N-1} = z_N$. We collect all the nodal values in the vector $\boldsymbol{P} = \{r_1, z_1, r_2, z_2, \ldots, r_N, z_N\}$. If local inextensibility is required, we need to discretize the field of Lagrange multipliers

$$\lambda(u) \approx \sum_{J=1}^{M} \hat{B}_J \lambda_J,$$

where $\hat{B}_J$ are taken here to be the quadratic B-Splines obtained from the same knot vector used to generate the functions B_I.

Plugging these representations into the different models, generically written as

$\mathcal{L}$, and equating to zero the derivatives of $\mathcal{L}$ with respect to the control points $\{r_I(t), z_I(t)\}$, possibly λ_J and the global multipliers $\mathbf{\Lambda}$ (or equivalently evaluating the variations in equation (3.4) at the B-Spline basis functions), the Galerkin semi-discrete equations follow as

$$\begin{aligned} \mathbf{D}(\boldsymbol{P})\dot{\boldsymbol{P}} + \mathbf{L}(\boldsymbol{P})\boldsymbol{\lambda} &= \boldsymbol{f}(\boldsymbol{P}) \\ \mathbf{L}^T(\boldsymbol{P})\dot{\boldsymbol{P}} &= \mathbf{0} \end{aligned} \tag{4.3}$$

where $\boldsymbol{\lambda}$ collects all the Lagrange multipliers for a given model. This system of differential-algebraic equations is integrated in time with a specialized package.

Specifically, recalling equation (3.5), the entries for column of the constraint matrix $\mathbf{L}$ corresponding to the global volume constraint are

$$L_{Ir}^{\text{vol}} = -D^{\text{vol}}[B_I, 0], \quad L_{Iz}^{\text{vol}} = -D^{\text{vol}}[0, B_I].$$

Similarly, recalling equation (3.6), the column of $\mathbf{L}$ corresponding to the global area constraint is

$$L_{Ir}^{\text{area}} = -D^{\text{area}}[B_I, 0], \quad L_{Iz}^{\text{area}} = -D^{\text{area}}[0, B_I].$$

The matrix entries corresponding to the local inextensibility constraints are

$$L_{Ir,J}^{\text{inext}} = -\int_0^1 \left(\frac{r'}{a^2} - \frac{Hz'}{a}\right) B_I \hat{B}_J (2\pi a r)\mathrm{d}u, \; L_{Iz,J}^{\text{inext}} = -\int_0^1 \left(\frac{z'}{a^2} + \frac{Hr'}{a}\right) B_I \hat{B}_J (2\pi a r)\mathrm{d}u.$$

Recalling equation (3.10), the elastic force vector is computed as

$$f_{Ir} = G[B_I, 0], \quad f_{Iz} = G[0, B_I].$$

From equation (3.7), it follows that the only nonzero entries of $\mathbf{D}^{\text{mem}}$ are

$$D_{Ir,Jr}^{\text{mem}} = \int_0^1 \mu B_I B_J \frac{8\pi a}{r}\mathrm{d}u.$$

4.3 The Bulk Dissipation Matrix $\mathbf{D}^{\text{bulk}}$

We discretize the ambient velocity field and pressure as

$$\boldsymbol{u} \approx \sum_a N_a \boldsymbol{u}_a, \qquad p \approx \sum_b \hat{N}_b p_b.$$

To enforce the no slip condition, we define

$$\Pi = \int_\Gamma |\boldsymbol{V} - \boldsymbol{u}|^2 \, \mathrm{d}S,$$

which we minimize with respect to $\dot{\boldsymbol{P}}_I$ to find the relation

$$\mathbf{M}\dot{\boldsymbol{P}} = \mathbf{N}\boldsymbol{U}, \tag{4.4}$$

where $\boldsymbol{U} = \{u_{1r}, u_{1z}, u_{2r}, u_{2z}, \ldots, u_{nr}, u_{nz}\}$ and

$$M_{IiJj} = \delta_{ij} \int_\Gamma B_I B_J \mathrm{d}S, \qquad N_{Iiak} = \delta_{ik} \int_\Gamma B_I N_a \mathrm{d}S.$$

The lower-case indices i, j and k run over r and z.

After standard space discretization, the discrete equations for the bulk flow take the form

$$\begin{aligned} \mathbf{K}\boldsymbol{U} + \mathbf{L}_p \boldsymbol{p} &= \mathbf{N}^T \mathbf{M}^{-1} \boldsymbol{f}(\boldsymbol{P}) \\ \mathbf{L}_p^T \boldsymbol{U} &= \mathbf{0} \end{aligned} \tag{4.5}$$

The form of the forcing term follows from the power conjugacy between $\dot{\boldsymbol{P}}$ and $\boldsymbol{f}$, together with equation (4.4). Isolating $\boldsymbol{U}$ from the first equation in (4.5) and plugging it into the second equation allows us to write

$$\boldsymbol{p} = (\mathbf{L}_p^T \mathbf{K}^{-1} \mathbf{L}_p)^{-1} \mathbf{L}_p^T \mathbf{K}^{-1} \mathbf{N}^T \mathbf{M}^{-1} \boldsymbol{f}.$$

Replacing back in the first equation, and recalling equation (4.4), we find

$$\dot{\boldsymbol{P}} = \underbrace{\mathbf{M}^{-1}\mathbf{N}\left(\mathbf{K}^{-1} - \mathbf{K}^{-1}\mathbf{L}_p(\mathbf{L}_p^T\mathbf{K}^{-1}\mathbf{L}_p)^{-1}\mathbf{L}_p^T\mathbf{K}^{-1}\right)\mathbf{N}^T\mathbf{M}^{-1}}_{(\mathbf{D}^{\text{bulk}})^{-1}}\boldsymbol{f}$$

In a pure Dirichlet problem, the pressures are defined up to a constant. Taking a solution and adding a constant to the pressure field clearly shows from the equations that it is also a solution. In order to remove this the indeterminacy, we applied a constraint on the bulk pressure

$$\sum_n p_n = 0$$

This constraint introduces another Lagrange multiplier to the system which leads to an additional equation and more complex bulk dissipation matrix.

$$\begin{aligned} \mathbf{K}\boldsymbol{U} + \mathbf{L}_p\boldsymbol{p} &= \mathbf{N}^T\mathbf{M}^{-1}\boldsymbol{f}(\boldsymbol{P}) \\ \mathbf{L}_p^T\boldsymbol{U} + \mathbf{L}_s\gamma &= \mathbf{0} \\ \mathbf{L}_s^T\boldsymbol{p} &= 0 \end{aligned} \tag{4.6}$$

where $\mathbf{L}_s$ is a vector of ones. By solving for Lagrange multipliers in second and third equation and replacing back in the first equation, the bulk matrix is found

$$\mathbf{D}^{\text{bulk}} = \left\{\mathbf{M}^{-1}\mathbf{N}\left[\mathbf{K}^{-1} - \mathbf{K}^{-1}\mathbf{L}_p(\mathbf{L}_p^T\mathbf{K}^{-1}\mathbf{L}_p)^{-1}\mathbf{L}_p^T\mathbf{K}^{-1} + \mathbf{H}\right]\mathbf{N}^T\mathbf{M}^{-1}\right\}^{-1}$$

where

$$\mathbf{H} = \mathbf{K}^{-1}\mathbf{L}_p(\mathbf{L}_p^T\mathbf{K}^{-1}\mathbf{L}_p)^{-1}\mathbf{L}_s(\mathbf{L}_s^T(\mathbf{L}_p^T\mathbf{K}^{-1}\mathbf{L}_p)^{-1}\mathbf{L}_s)^{-1}\mathbf{L}_s^T(\mathbf{L}_p^T\mathbf{K}^{-1}\mathbf{L}_p)^{-1}\mathbf{L}_p^T\mathbf{K}^{-1}$$

This type of formulation for bulk dissipation is very important because it allows us to combine different dissipation mechanisms, easily, by adding two different dissipation matrix.

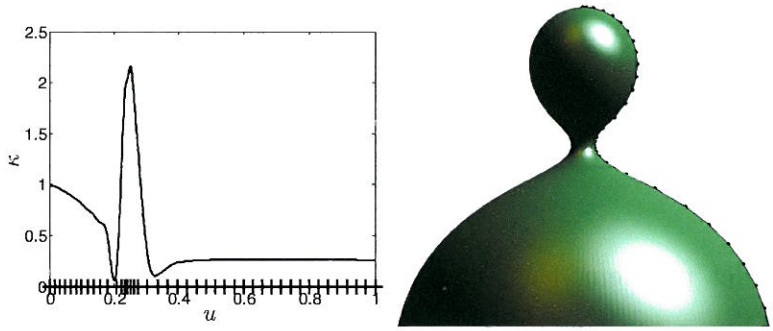

Figure 4.1: Non-uniform knot span adapted to the curvature of the generating curve (left), and control polygon for a given vesicle shape (right).

4.4 Reparametrization

The B-Spline curve, which represent the desired biological membrane, described in equation 4.1 is obtained by integrating the velocity of the control points of generating curve ($\boldsymbol{P}$) in time. Therefore, there is no restriction on the relative position of the control points and this may cause clustering of the control points in some areas irrespective of the geometric features of the generating curve and leads to over-resolving of some areas while some other areas have poor resolution. Furthermore, the curvatures of the B-Spline is changing during the time, and considering that higher curvature parts need more resolution to be represented accurately, it is important to re-parametrize the generating curve periodically in the simulations.

Here, we have devised a combination of two different re-parametrization methods: Arc-length re-parametrization (Peterson and Taligent, 2006; Sharpe and Thorne, 1982), in order to avoid control points getting too close and cross over each other, and curvature-based re-parametrization, to capture higher curvatures more accurately.

This combined re-parametrization method builds a non-uniform knot span for the B-Spline functions; hence, it clusters the knots where the curvature of the generating curve is high while avoiding too close control points. At the re-parameterization instants, the new control points relative to the new set of basis functions are obtained by a least square fit to the previous description of the generating curve that results in a nearly arc-length parameterization, see figure 4.1 for an illustration. This method

allows us to significantly reduce the number of control points as compared to resolving the fine geometrical features with uniform refinement, and still obtain very accurate solutions.

Chapter 5

Simulation Results

5.1 Introduction

In this section, first, the results for a simple yet informative axisymmetrical example is introduced and compared with the available analytical solution in order to verify the applied numerical method and investigate the boundary effects. Then, the dynamic simulations of a biological membrane are illustrated with focus on the evolution of curvature energy during time for a sufficiently large and fine mesh.

5.2 Biomembrane Dynamic Simulation Results

In this simulation, we start with an out-of-equilibrium membrane, which is represented with a cubic B-Spline, and continue solving the system of equations, described in Chapter 4, until the system reaches an equilibrium state. The novel numerical technique explained in Chapter 4 is applied here. As mentioned before, this combined immersed finite element B-Spline method requires a background finite element mesh. Figure 5.1 shows the whole adaptive background mesh and the B-Spline curve. Q2/Q1 elements have been used in order to satisfy LBB condition. Figure 5.2 shows a closer look of the mesh near the B-Spline. The position of control points in the elements is illustrated in figure5.3.

Chapter 6

Conclusions

Motivated by the out-of-equilibrium behavior of systems in biology and bio-inspired technology, I have studied, computationally, the dynamics of biological membranes with a particular emphasis on development of a novel numerical technique, Finite Element Immersed Boundary (FEIB) method.

In the presented work, first the composition and structure of biological membranes have been explained and the physical role of lipids, as the main component of all biomembranes, on fluidity and bilayer formation of membranes has been discussed. Then, a continuum model for an inextensible fluid membrane with curvature elasticity immersed in a viscous, incompressible Newtonian fluid has been described and after that based on this model and B-Spline curve representation a special semi-discretization with related bulk dissipation matrix was derived. Finally, some dynamic simulations of a biological membrane was presented, reliability of the introduced re-parametrization method was investigated and the numerical method was verified by means of available analytical solution for the most important example of axisymmetrical flow.

The new formulation of bulk dissipation matrix empower us to combine bulk dissipation with other dissipation models which are effective in different biomembranes. This is very important because although for large vesicles, the bulk viscosity plays an important role to set the dynamics, for small vesicles, curvature energy and membrane viscosity become dominant driving and dissipative mechanisms (Arroyo and DeSimone, 2009) which is common in cell biology and in man-made bio-inspired sys-

Dimova, R., S. Aranda, N. Bezlyepkina, V. Nikolov, K. A. Riske, and R. Lipowsky (2006, Jul). A practical guide to giant vesicles. probing the membrane nanoregime via optical microscopy. *Journal of Physics: Condensed Matter 18*(28), S1151–S1176.

Du, Q., C. Liu, R. Ryham, and X. Wang (2009). Energetic variational approaches in modeling vesicle and fluid interactions. *Physica D 238*, 923–930.

Du, Q., C. Liu, and X. Wang (2006). Simulating the deformation of vesicle membranes under elastic bending energy in three dimensions. *Journal of Computational Physics 212*, 757–777.

Gurtovenko, A. and I. Vattulainen (2005). Pore formation coupled to ion transport through lipid membranes as induced by transmembrane ionic charge imbalance: atomistic molecular dynamics study. *J. Am. Chem. Soc 127*(50), 17570–17571.

Happel, J. and H. Brenner (1983). *Low Reynolds Number Hydrodynamics: with special applications to particulate media.* Martinus Nijhoff Publishers.

Heltai, L. (2008). On the stability of the finite element immersed boundary method. *Computers & Structures 86*(7-8), 598–617.

Hughes, T., J. Cottrell, and Y. Bazilevs (2005). Isogeometric analysis: CAD, finite elements, NURBS, exact geometry and mesh refinement. *Computer Methods in Applied Mechanics and Engineering 194*(39-41), 4135–4195.

Israelachvili, J. (1991). *Intermolecular and surface forces.* Academic press London.

Kessel, R. and R. Kardon (1979). *Tissues and organs: a text-atlas of scanning electron microscopy.* WH Freeman San Francisco.

Liu, W., T. Belytschko, and H. Chang (1986). An arbitrary lagrangian-eulerian finite element method for path-dependent materials* 1. *Computer Methods in Applied Mechanics and Engineering 58*(2), 227–245.

Liu, W., D. Kim, and S. Tang (2007). Mathematical foundations of the immersed finite element method. *Computational Mechanics 39*(3), 211–222.

Liu, W., Y. Liu, D. Farrell, L. Zhang, X. Wang, Y. Fukui, N. Patankar, Y. Zhang, C. Bajaj, J. Lee, et al. (2006). Immersed finite element method and its applications to biological systems. *Computer methods in applied mechanics and engineering 195*(13-16), 1722–1749.

Lodish, H., A. Berk, C. A. Kaiser, M. Krieger, M. P. Scott, A. Bretscher, H. Ploegh, and P. Matsudaira (2003). *Molecular Cell Biology.* W.H.Freeman.

Marsden, J. and T. Hughes (1983). *The mathematical foundations of elasticity.* Prentice-Hall.

Mittal, R. and G. Iaccarino (2005). Immersed boundary methods.

Mohammadi, S. (2008). *Extended finite element method.* Oxford: Blackwell Publishing.

Peskin, C. (1972, October). Flow patterns around heart valves: A numerical method. Volume 10, pp. 252–271.

Peskin, C. (2003). The immersed boundary method. *Acta Numerica 11*, 479–517.

Peterson, J. and I. Taligent (2006). Arc Length Parameterization of Spline Curves.

Piegl, L. and W. Tiller (1997). *The NURBS book.* Springer Verlag.

Reynwar, B. J., G. Illya, V. A. Harmandaris, M. M. Mueller, K. Kremer, and M. Deserno (2007). Aggregation and vesiculation of membrane proteins by curvature-mediated interactions. *Nature 447*(7143), 461–464.

Saffman, P. G. and M. Delbruck (1975). Brownian Motion in Biological Membranes. *Proceedings of the National Academy of Sciences 72*(8), 3111–3113.

Scriven, L. (1960). Dynamics of a fluid interface: equations of motion for newtonian surface fluids. *Chem. Eng. Sci. 12*, 98–108.

Seifert, U. and R. Lipowsky (1995). *Handbook of Biological Physics*, Volume 1, Chapter Morphology of Vesicles. Elsevier Science B.V.

Sharpe, R. and R. Thorne (1982). Numerical method for extracting an arc length parameterization from parametric curves. *Computer-Aided Design 14*(2), 79–81.

Shillcock, J. and R. Lipowsky (2006). The computational route from bilayer membranes to vesicle fusion. *Journal of Physics: Condensed Matter 18*, S1191–S1219.

Simonett, G. (2001). The Willmore flow near spheres. *Differential Integral Equations 14*(8), 1005–1014.

Sprong, H., P. van der Sluijs, and G. van Meer (2001). How proteins move lipids and lipids move proteins. *Nature Reviews Molecular Cell Biology 2*(7), 504–513.

Stone, H. and A. Ajdari (1998). Hydrodynamics of particles embedded in a flat surfactant layer overlying a subphase of finite depth. *J. Fluid Mech. 369*, 151–173.

Wagner, G., N. Moes, W. Liu, and T. Belytschko (2001). The extended finite element method for rigid particles in Stokes flow. *International Journal for Numerical Methods in Engineering 51*(3), 293–313.

Zhang, L., A. Gerstenberger, X. Wang, and W. Liu (2004). Immersed finite element method* 1. *Computer Methods in Applied Mechanics and Engineering 193*(21-22), 2051–2067.

Zhilin, L. (1998). The immersed interface method using a finite element formulation. *Applied Numerical Mathematics 27*(3), 253–267.